AIAA SciTech Forum
8-12 January 2024, Orlando, FL
AIAA SCITECH 2024 Forum

10.2514/6.2024-2706

A Comparative Study of Continuous-Wave and Pulsed Operation of Rotating Magnetic Field Thrusters for Plasma Propulsion

Tate M. Gill *, Christopher L. Sercel *, Grace Zoppi *, and Benjamin A. Jorns †
University of Michigan, Plasmadyamics and Electric Propulsion Laboratory, Ann Arbor, MI, 48109

The performance of a rotating magnetic field (RMF) thruster in pulsed and continuous wave (CW) operation is experimentally evaluated. A suite of far-field probes is employed to characterize both the overall jet efficiency in addition to the contributions of individual phenomenological efficiency modes at a power level of 10 kW. It is found that the efficiency of the RMF thruster in CW mode, 2.9%, is approximately four times higher than in pulsed mode with the same power, flow rate, and applied magnetic field. Further measurements on coupling efficiency, mass utilization, plasma efficiency, and divergence efficiency show an average improvement of 155% in CW mode for each efficiency metric. The largest enhancement comes from the plasma efficiency, a metric of the conversion of power absorbed by the plasma to the kinetic power in the exhaust, which rises from 7.6% in pulsed mode to 13.5% in CW mode. This result reinforces the hypothesis that there is an intrinsic inefficiency of RMF thrusters in pulsed mode stemming from the thrust transfer mechanism. Despite these improvements, the overall efficiency of RMF thrusters remains below the efficiency of state-of-the-art electric propulsion. The work posits that focusing on CW mode enhancements could further improve RMF thruster performance.

I. Introduction

Electric propulsion (EP) is a maturing field now dominated by Hall effect (HET) and gridded ion thrusters (GIT). These plasma devices allow spacecraft to efficiently use propellant by delivering much higher specific impulse than is capable via chemical rockets. Although widely employed for both low-earth and geo-synchronous orbits, these thrusters are not currently suitable for next-generation high power EP missions, such as rapid transits to cislunar space or very-low air-breathing orbits. Given the growing interest in both high-power and molecular-propellant EP applications, the development of advanced concept electric propulsion architectures is required to address these needs.

Once such concept is inductive plasma propulsion, wherein power transfer occurs through the use of time-varying magnetic fields which eliminates the need for the current carrying plasma-wetted electrodes inherent to the operation of HETs and GITs. These electrodes, particularly thermionic emitting cathodes, pose life-time concerns when operated on reactive molecular propellants. To date, inductive propulsion has successfully demonstrated competitive performance on alternative propellants [1]. However, this previous thruster architecture was practically limited by the need to use high voltage pulses (30-60 kV) and pulsed gas valves, which hinders their adoption for flight missions. An alternate inductive thruster concept to this—and the subject of this work—is the rotating magnetic field (RMF) thruster which aims to address the limitations of similar in-family thrusters though the use of a unique current drive method. This mechanism allows for significantly lower peak voltages on the order of 100's of volts.

Given this advantage, there have been several efforts to develop RMF thruster technology. However, past efforts have struggled to achieve competitive propulsive efficiencies. Measured results to date exhibit performances typically below 1% [2–5]. These efforts all employ pulsed RMF systems, where an initial mass-bit of propellant is ionized and accelerated by the RMF during a short-duration pulse typically between 100 μs and 1 ms. Previous work by Gill et al. [6] showed that pulsed mode operation suffers from excessive initial gas density leading to large energetic losses to excitation radiation as well as to the walls within the thruster.

Given the lower voltages required in RMF thrusters there is an opportunity to explore their operation in a continuous-wave (CW) mode. In this framework, the RMF is applied to the plasma for substantially longer times than typical neutral particle transits (>1 s). In this mode there is no build up of neutral density between pulses. In theory, this leads to higher mass throughput at lower densities, which directly corresponds to higher average thrust, specific impulse, and increased efficiency for these devices. The validity of this hypothesis about improved performance under CW conditions has yet

*Ph.D. Candidate, Department of Aerospace Engineering, University of Michigan, Ann Arbor, MI. AIAA Student Member
†Associate Professor, Department of Aerospace Engineering, University of Michigan, Ann Arbor, MI. AIAA Associate Fellow

to be experimentally verified, but our previous theoretical work suggests an efficiency increase of 2-3 times present performance [7].

With this in mind, the goal of this work is to explore CW operation of RMF thrusters and compare the efficiency to typical pulsed thruster operation. To this end, this paper is organized as follows: in section II we describe the method of operation of RMF thrusters and outline the pertinent physics that distinguishes CW from pulsed operation. In section III, we provide a description of the RMF thruster test article and the experimental setup. Following this, we define the terms in our phenomenological efficiency model for RMF thrusters and describe the diagnostic probes and methods used to evaluate them. In section IV, we report the measurements from our diagnostic probes, and using these results we evaluate probe-measured component efficiencies from the efficiency model. In section V we discuss these results to provide context for future thruster operation and design. Finally, in section VI we summarize the findings of this work and orient these results in relation to the broader field of electric spacecraft propulsion.

II. Theory

In this section we provide a simplified description of the operation of RMF thrusters to orient the reader and justify the hypotheses that underpin this work.

A. RMF Operational Principles

The core of an RMF thruster is a series of antennas oriented transverse to the axis of the thruster. During operation, these coils carry electric currents in-phase corresponding to their geometric location. For example, in this work we employ a three-phase RMF system with coils oriented 120 degrees from each other that operate with a 120 degree electrical phase offset. This setup produces the rotating magnetic field which travels about the thruster at the same frequency as the alternating currents through the antennas. Surrounding the RMF antennas are a series of DC bias coils that produce a steady magnetic field that assists with plasma confinement and acceleration. If we assume a perfectly uniform RMF the resulting magnetic field takes the form:

$$B_r = B_\omega \cos(\omega t - \theta) + B_r^0 \tag{1}$$

$$B_\theta = B_\omega \sin(\omega t - \theta) \tag{2}$$

$$B_z = B_z^0, \tag{3}$$

where B_ω is the amplitude of the RMF, ω is the angular frequency, B_r^0 and B_z^0 are the steady field components produced by the bias magnets, conductive structures, and the plasma currents, and t, r, z, and θ are the time, radial, axial, and angular coordinates respectively. In the case of axial symmetry—change is θ much weaker than change in z—the time-varying RMF generates an axial electric field by Faraday's Law of the form

$$E_z = \omega r B_\omega \cos(\omega t - \theta) + E_z^0, \tag{4}$$

where E_z^0 is a steady axial field that is responsible for ion acceleration. Typically this electric field is not sufficiently strong to initiate plasma breakdown in a neutral gas, but when produced in the presence of initial seed electrons, the alternating electric field drives further ionization. Subsequently, when a plasma forms, this axial electric field acts in-phase with the radial component of the RMF field to drive a steady azimuthal electron current,

$$v_\theta = \frac{E_z B_r}{|B|^2}, \tag{5}$$

where, $|B|$ is the magnitude of the total magnetic field, and we have neglected pressure gradient and collisional drag forces. This expression in general is a function of azimuthal position; however the steady phase-averaged values shown to be [**?**]

$$v_\theta = \omega r \tag{6}$$

$$E_z^0 = v_\theta B_r^0. \tag{7}$$

The interplay between the bias magnetic field and the RMF to produce these illustrative equations is complex and requires numerical methods to solve explicitly. The general equations presented above (Eqns. 6 and 7) are sufficient

to explain the operational principle of the thruster; importantly, this expression only holds in the limit of high RMF strength relative to other magnetic fields and forces.

B. RMF Modes

In this work we operate the thruster in two differing modes to compare the performance. The first is pulsed mode, which consists of short high-amplitude application of the RMF. This translates to driving currents on the order of 500 A peak, over pulse lengths on the scale of 100 μs. This mode has two primary advantages: first, it provides higher RMF strength to drive the requisite azimuthal electron currents and ionize the propellant, and second, it allows for time varying currents to form in conductive structures on the engine which drives quadratic thrust scaling with the driven current. We show in Fig. 1b an image of the RMF thruster operating in pulsed mode.

The second mode we investigate is continuous wave (CW) mode, in which the RMF is applied consistently to the plasma at 100% duty cycle. For a constant power, this necessarily results in a lower RMF amplitude. In our case this translates to peak RMF currents on the order of 100 A. In this mode we lose the advantage of quadratic thrust scaling as the currents in the plasma will not significantly vary in time. However, this mode has the advantage of applying a constant force to the plasma which should result in higher average exit velocities. Furthermore, via continuity the higher average velocity should produce a lower density plasma which reduces inelastic collisional losses. We show in Fig. 1a an image of the RMF thruster operating in CW mode.

(a) 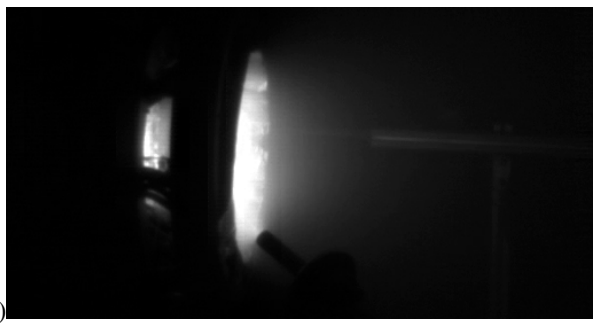 (b) 

Fig. 1 High speed camera images taken of the thruster firing in (a) CW mode, and (b) pulsed mode.

C. Phenomenological Efficiency Model

Here we define a phenomenological efficiency model to assess the performance of both CW and pulsed mode operation. This model takes into account various efficiency parameters to provide a comprehensive comparison between the two modes. To this end, we can write the jet efficiency of a thruster as

$$\eta = \frac{T^2}{2\dot{m}P_{in}}, \tag{8}$$

where, T is the thrust produced, $\dot{m}$ is the neutral mass flow rate, and P_{in} is the input power. We can break this expression into component efficiency factors in the model as follows:

$$\eta = \eta_m \eta_d \eta_c \eta_p \tag{9}$$

where, η_m is the mass utilization efficiency, η_d is the divergence efficiency, η_c is the coupling efficiency, and η_p is the plasma efficiency. Using this phenomenological efficiency model and our definitions of component efficiency terms, we have a framework to evaluate the overall efficiency of our test article. The goal of the following experiment is to evaluate the contributions of the component efficiency modes of the RMF test article operating in both pulsed and CW modes using plasma diagnostic techniques. Below, we provide physical interpretation for the these component efficiency modes and define them explicitly.

1. Mass Utilization Efficiency

Mass utilization efficiency quantifies how effectively the propellant mass is ionized and therefore able to be acted upon by the electromagnetic forces produced by the thruster. It is defined as

$$\eta_m = \frac{\dot{m}_i}{\dot{m}}, \tag{10}$$

where $\dot{m}_i$ is the mass flow rate of ions in the beam.

2. Divergence Efficiency

Divergence efficiency characterizes the ability of the thruster to collimate the accelerated plasma ions into a narrow beam, reducing losses due to radially directed momentum which symmetrically cancels. Divergence efficiency is defined as

$$\eta_d = \left(\frac{I_a}{I_b}\right)^2, \tag{11}$$

where I_a and I_b are the axial and total ion current from the thruster respectively.

3. Coupling Efficiency

Coupling efficiency quantifies the effectiveness of the energy transfer from the RMF power system to the plasma. This mode is a measure of parasitic losses in the formation of the rotating magnetic field relative to the effective load of the plasma. Coupling efficiency is defined as

$$\eta_c = \frac{P_p}{P_{in}}, \tag{12}$$

where P_p is the power into the plasma and P_{in} is the power into the RMF power processing unit.

4. Plasma Efficiency

Lastly, plasma efficiency represents the ratio of the total beam power of the accelerated ions to the power coupled to the plasma by the RMF. It accounts for the overall energy conversion efficiency of the thruster. Plasma efficiency is defined as

$$\eta_p = \frac{I_b\langle\varepsilon\rangle}{P_p}, \tag{13}$$

where the beam power is written as $P_{beam} = I_b\langle\varepsilon\rangle$ and $\langle\varepsilon\rangle$ is the average ion kinetic energy.

III. Methods

In this section we provide an overview of the RMF test article, as well as describe the experimental setup, test conditions, and diagnostic probes utilized in this study.

A. Experimental Setup and Test Article

These experiments were conducted at the University of Michigan's Plasmadynamics and Electric Propulsion Laboratory (PEPL) in the Alec D. Gallimore Large Vacuum Test Facility. This cylindrical vacuum chamber measures 6 m in diameter and 9 m in length and has a maximum xenon pumping speed of 600 kL/s. During these experiments the chamber pressure was on the order of 1e-6 Torr-xenon as measured by a ion gauge mounted on the chamber wall.

We show in Fig. 2 the test article we investigate in this work; the PEPL RMFv3 thruster. This thruster employs three double-turn Helmholtz-pair antennas which are powered by a custom three-phase resonant sine inverter to produce the approximately 400 kHz RMF. The thruster body consists of a blown glass nozzle which follows the shape of the steady magnetic field. The body has a 14 cm initial diameter, a 25 cm exit diameter, and is ~15 cm long. The steady magnetic field is primarily produced by the main bias electromagnet located at the throat of the thruster (right most electromagnet seen in Fig. 2a). An additional trim magnet is located downstream at the thruster exit and serves to tailor the shape of

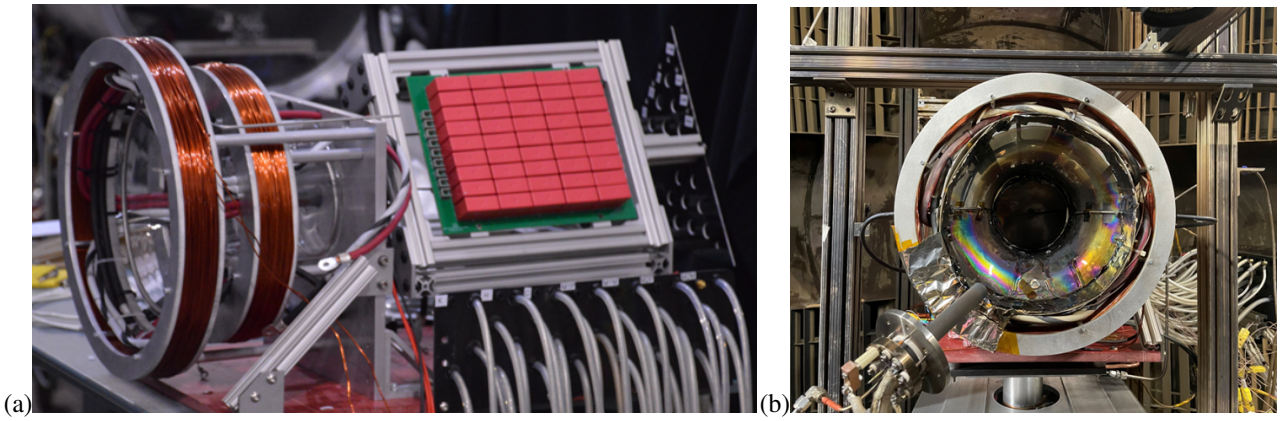

Fig. 2 PEPL RMFv3 thruster. (a) image taken during assembly (b) image taken after experiment

Parameter	CW	Pulsed
Injector Location	Throat	Wall
Injector Mass Flow	257 sccm Xe	257 sccm Xe
Cathode Flow	15 sccm Xe	15 sccm Xe
Cathode Current	3 A	3 A
RMF Power	10.3 ± 0.7 kW	10.5 ± 0.7 kW
RMF Frequency	415 kHz	415 kHz
Pulse Length	10 s	200 μs
Duty Cycle	100 %	7.8 %
Pulse Frequency	-	390 Hz

Table 1 Thruster settings for the CW and Pulsed operating conditions.

the magnetic field in-situ. The thruster has two neutral injectors that are fed from independent mass flow controllers. The first annular injector is placed at the throat of the thruster facing downstream, and the second is a pair of injectors located at 3 and 9 o'clock along the thruster wall which produce flow tangentially opposing the motion of the RMF. The thruster is also outfitted with a 20 A-class LaB6 hollow cathode pointed into the thruster along the magnetic field to act as a seed ionization source. We operate the cathode at a steady 3 A keeper current at 15 sccm xenon. As will be shown in Sec. IV, this current is not related to the beam current produced by the thruster and in theory could be replaced by an inductively-coupled radio-frequency or helicon source. We choose to use a thermionic hollow cathode for reliability and ease of implementation.

In Table 1 we report the thruster settings for the two operating modes. These were selected for performance comparison at approximately the same overall RMF power, bias magnetic field, and flow rate. The notable exception is that we exclusively use the throat injector for the CW mode, and exclusively use the wall injector for the pulsed mode. This choice is motivated by a consistent increase in efficiency seen for the respective mode-injector pairs during initial path-finding performance measurements.

B. Diagnostics

In this study, we employ a comprehensive set of plasma and thruster diagnostics to investigate the plasma characteristics and performance of the RMF thruster in both CW and pulsed mode. We show in Fig. 3 the locations of these tools within the vacuum facility. The following diagnostics are utilized:

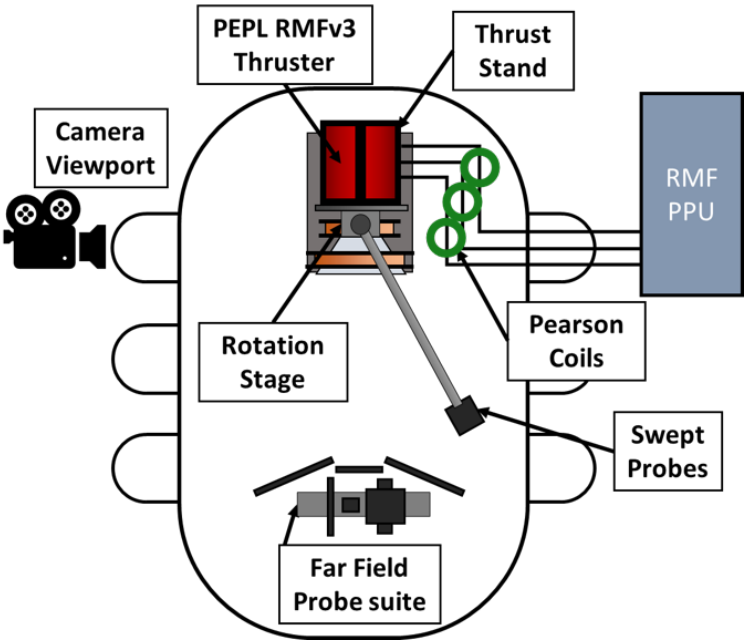

Fig. 3 Location of diagnostics within vacuum facility. RPA is located in the far-field probe suite, FP is included in the swept probes on the radial arm, and the Pearson coils are located between the RMF antennas and the resonant capacitor banks behind the thruster.

1. Pearson Coils

Three wide-band Pearson coils are placed around the conductors of each antenna phase behind the thruster and between the antenna and the resonant capacitor bank. These are used to measure the currents through each antenna for resonance tuning and the evaluation of coupling efficiency.

2. Swept Faraday Probe

A swept Faraday probe (FP) is employed to measure the far-field ion flux throughout the plume. The probe is moved through the plasma beam to obtain spatial profiles of ion current density. The FP used in this work consists of a 1.74 cm molybdenum collector surrounded by an annular 0.54 cm molybdenum guard ring with a 0.05 cm gap between them. Both the collector and guard are biased to -60 V relative to facility ground to ensure that ion saturation is achieved.

3. Retarding Potential Analyzer

A retarding potential analyzer (RPA) is used to measure the ion energy distribution in the plume downstream of the thruster. The RPA used in this work consists of four grids. In order for the incident plasma these are: a floating attenuation grid, an electron suppression grid biased to -30 V, an ion selection grid swept from 0 - 100 V, and a secondary electron suppression grid also biased to -30 V. Following the grids there is a collector electrode which we bias to -5 V. The RPA is aligned to thruster centerline at a distance of approximately 2 m from the thruster exit plane. Typically, a far-field Langmuir probe is used to measure the local plasma potential to correct for the fact that the ion selection grid is biased with respect to ground. However, due to the radio-frequency noise produced by the thruster an accurate measure of the plasma potential has not been performed. We do note however that the plasma potential for Hall thrusters operating at a similar power level are on the order of 5 V [8], and therefore the associated error in our reported measurements should be relatively small.

IV. Results

We collected experimental data for the CW and pulsed mode operation of the RMF thruster. The collected data are analyzed to calculate the efficiency parameters and assess the thruster performance in each mode. In this section we outline the procedures and equations used to convert our probe measurements to the component efficiency modes.

Unless otherwise noted, we report as the uncertainty a standard 95% confidence interval from the standard error of multiple independent measurements.

A. Coupling Efficiency

Using the Pearson coils to measure the currents through the RMF antennas, we assess the coupling efficiency of the thruster. As stated previously, the coupling efficiency is defined as the ratio of input power to power coupled into the plasma through the RMF system. The input power is measured as the product of the DC voltage and DC current supplied to the RMF PPU and we take a conservative 5% uncertainty for both these measurements. The imput power is shown in Table 1 for the two modes. The coupled plasma power can be evaluated by measuring an effective circuit resistance with and without the plasma present. The effective resistance for a given case can be written as

$$R = \frac{P_{in}}{\sum_k \bar{I_k^2}}, \tag{14}$$

where the sum is taken over the number of phases (three in our case), P_{in} is the input DC power, and $\bar{I_k^2}$ is the time-averaged squared current through antenna phase k. This equation is analogous to the AC power deposited in an resistor $P = RI_{rms}^2$, where I_{rms} is the root-mean-squared current. With the thruster unloaded we find an effective vacuum resistance of $R_{CW,v} = 612 \pm 31$ mΩ for the CW mode, and $R_{Pulsed,v} = 657 \pm 50$ mΩ for the pulsed mode. These values are quite close to each other and are within uncertainty. This is expected as the driving circuit does not differ between modes, and the slight increase in resistance for the pulsed mode is consistent for a current-dependent resistance increase for the IGBT semiconducting switches used in the PPU.

Repeating this process for the currents measured during thruster operation yields a plasma-loaded effective resistance of $R_{CW,p} = 1097 \pm 78$ mΩ for the CW mode, and $R_{Pulsed,p} = 902 \pm 64$ mΩ for the pulsed mode. If we interpret the change in resistance as power coupled into the plasma, we can write an new expression for the coupling efficiency as

$$\eta_c = 1 - \frac{R_v}{R_p}, \tag{15}$$

where R_v is the vacuum effective resistance and R_p is the plasma-loaded effective resistance. By definition, the power coupled to the plasma is then $P_p = \eta_c P_{in}$. Using our calculated resistances, we arrive at a coupling efficiency of 44 ± 4% for the CW mode and 27 ± 3 % for the pulsed mode, with an associated plasma-coupled power of 4.5 ± 0.5 kW and 2.9 ± 0.4 kW respectively.

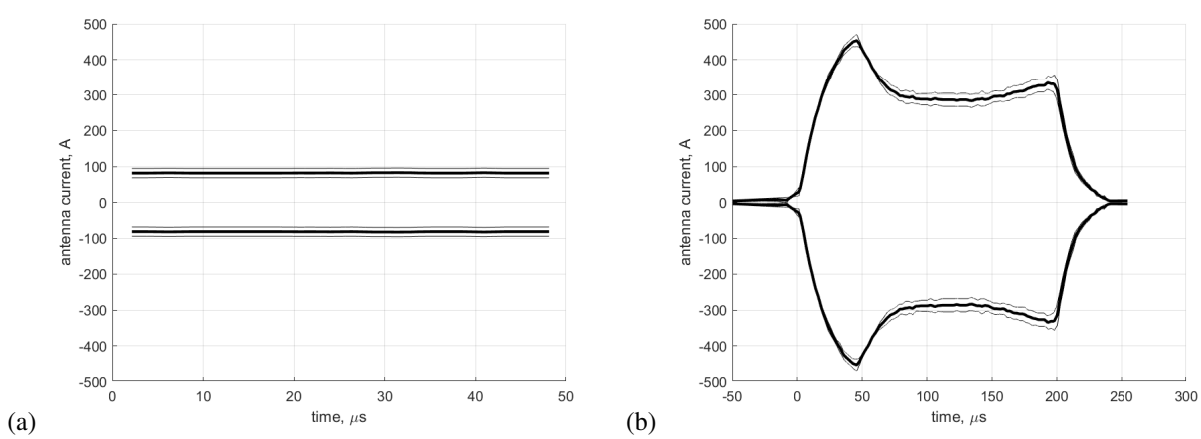

Fig. 4 Average RMF current envelopes of the three RMF phases for (a) CW mode and (b) pulsed mode. Shaded areas represent the range of current amplitudes for the three RMF phases.

These results show a notable increase in coupling efficiency for the CW mode, and the explanation is evident by looking at the plasma-loaded waveforms of RMF current. We show in Fig. 4 the average envelopes of the RMF currents with plasma present for the CW and pulsed modes. In the CW mode the current amplitude remains constant, which also indicates a constant power transfer to the plasma. However in the pulsed mode, the RMF current rises rapidly during the

first 50 μs of the pulse, settles to a semi-steady value at 100 μs, and then slowly rises until the end of the pulse at 200 μs. This behavior is indicative of the effective circuit resistance changing as a function of time. In the first 50 μs there is very little loading as the plasma is ionizing, and then coupling increases as the plasma forms, and then falls as the plasma is ejected. It is this initial startup time—where the circuit resistance is effectively equivalent to the vacuum case—that leads to a repeating energy loss every pulse and overall lower coupling efficiency in the pulsed mode.

B. Divergence and Mass Utilization

The Faraday probe (FP) provides us with the ion current density in the thruster plume. Utilizing these measurements as a function of polar angle about the thruster, we are able to calculate both the divergence efficiency and the mass utilization of the thruster. We show in Fig. 5 the ion current density measured with respect to the thruster centerline at a distance of 1.72 m from the thruster exit plane for both the CW and pulsed modes. The uncertainty for the CW mode (shaded area) is reported as the maximum current difference measured between two FP sweeps, and for the pulsed mode is reported as a 95% confidence interval from the standard deviation over 10 pulses. In the CW mode the ion current density is calculated from the collected probe current as

$$j(\theta) = \frac{I_{FP}(\theta)}{A_p + \kappa_G}\kappa_{SEE}, \tag{16}$$

where I_{FP} is the current collected from the FP, A_p is the probe collection area, and κ_G and κ_{SEE} are small geometric and secondary electron emission correction factors respectively [9]. However, for the pulsed mode, the probe measures the ion current density as a function of time, and we calculate the average effective ion current density as

$$j(\theta) = f_{rep}\int_0^{1/f_{rep}} j(\theta, t)dt, \tag{17}$$

where $j(\theta, t)$ is the ion current density as a function of time and position from Eq. 16 and f_{rep} is the pulse repetition rate. Turning to the measurements shown in Fig. 5 we can see that the CW mode results in a three times increase to centerline current density and a significantly more collimated beam. To generate quantitative metrics we can integrate over a supposedly symmetric hemispherical surface to calculate the total beam and axial beam currents respectively as

$$I_b = 2\pi r^2 \int_0^{\pi/2} j(\theta) sin(\theta) d\theta \tag{18}$$

$$I_a = 2\pi r^2 \int_0^{\pi/2} j(\theta) sin(\theta) cos(\theta) d\theta, \tag{19}$$

where $r = 1.72$ m is the radial distance to the FP. For the CW mode, we calculate a total beam current of 17.6 ± 1.2 A and an axial beam current of 12.4 ± 0.9 A. For the pulsed mode we calculate a total beam current of 13.3 ± 0.5 A and an axial beam current of 7.7 ± 0.3 A.

In typical fashion, we can relate these two terms to calculate the divergence efficiency as

$$\eta_d = \frac{I_a^2}{I_b^2}. \tag{20}$$

This leaves us with a divergence efficiency of 50 ± 7% for the CW mode and 33 ± 3% for the pulsed mode. The increased collimation we measure for the CW mode may be attributed to two mechanisms related to the higher density plasma in the pulsed mode. First, increased density will lead to larger thermal electron pressure forces in the plasma. These forces are likely to be highly isotropic and could result in the large measured divergence. Second, a higher plasma density will lead to larger azimuthal currents formed in the plasma. This increased current leads to increased magnetic pressure forcing the plasma to expand once it is no longer confined by the axial bias field provided by the thruster.

To calculate mass utilization, we need the relative charge states for the collected ions. Typically this is attained by a E×B Wein filter. The currents collected in E×B probes are usually on the order of pico to nano ampere's, and unfortunately the electromagnetic noise produced by the thruster makes these measurements infeasible. For this work, we assume all singly charged ions given that internal electron temperatures for RMF thrusters are typically low (~10 eV) [6]. With this assumption, we can then calculate mass utilization as

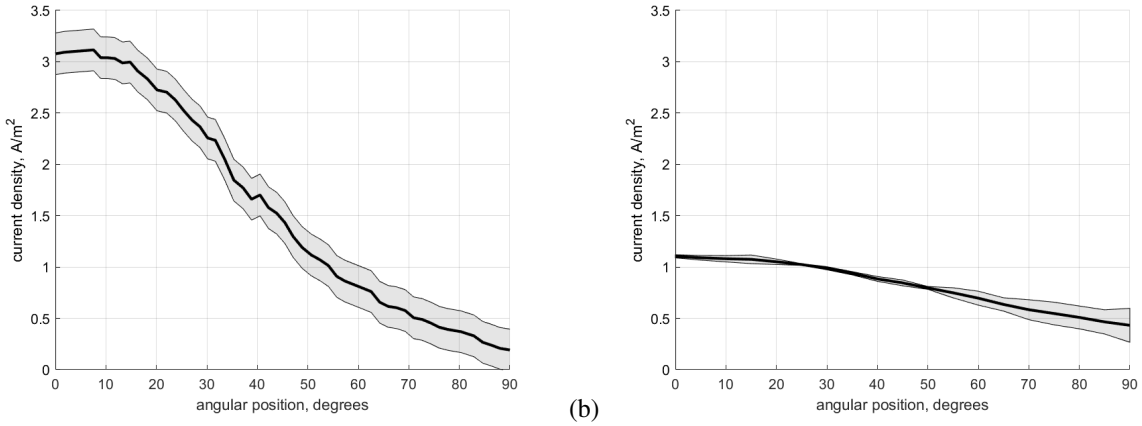

Fig. 5 Faraday probe measurements of ion current density in the thruster far-field for (a) CW mode, and (b) pulsed mode.

$$\eta_m = \frac{m_i I_b}{e\dot{m}}, \tag{21}$$

where, m_i is the ion mass, I_b is the total ion beam current, e is the elementary charge, and $\dot{m}$ is the neutral mass flow rate. This equation gives a mass utilization of 98 ± 12 % for the CW mode and 74 ± 8% for the pulsed mode. Here, again we see an increase in performance for the CW mode. We can attribute this increase directly to the increase in duty cycle between the two modes, and would expect that the pulsed mode would also exhibit very high mass utilization when operated at pulse repetition rates commensurate with the neutral refill time of the thruster (See Ref. [6]). However, this necessarily requires additional power to be supplied to the thruster.

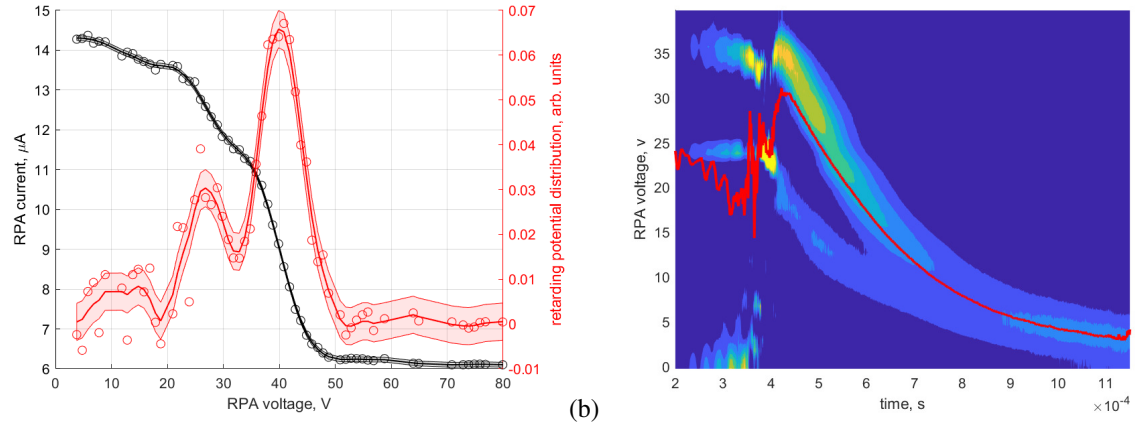

Fig. 6 RPA measurements on thruster centerline for (a) CW mode, and (b) pulsed mode.

C. Plasma Efficiency

To measure the plasma efficiency, we need to measure the kinetic energy of the ion beam. To this end, we employ a retarding potential analyzer situated along thruster centerline. This probe measures the retarding potential distribution of the ions—effectively a charge to mass energy distribution—, and we assume this distribution is uniform throughout the beam. We show in Fig. 6 the measured retarding potential distributions for the CW and pulsed modes. The black line in Fig. 6a shows the current measured by the RPA as a function of applied retarding voltage. The collected current consists of all ions with energy larger than the applied voltage, therefore we can calculate the original ion energy distribution function as

$$f(\varepsilon) \propto -\frac{dI_{RPA}}{dV}, \tag{22}$$

where I_{RPA} is the collected current by the RPA and V is the applied retarding voltage. We plot the resulting normalized energy distribution function for the CW mode in red in Fig. 6a. Additionally, we can calculate the mean ion energy as

$$\langle\varepsilon\rangle = \int_0^\infty f(\varepsilon)\varepsilon d\varepsilon. \tag{23}$$

For the CW mode this average ion energy is 35 ± 1 eV, and we can calculate the beam power as $P_{beam} = I_b\langle\varepsilon\rangle$. The resulting beam power is 620 ± 40 W.

For the pulsed mode, the analysis becomes more difficult as the ion energy and ion flux are both functions of time. We can perform the same procedure as outlined by Eqns. 22 and 23 for time-resolved ion current collection by the RPA. We show the resulting normalized ion energy distribution function over time in the color axis in Fig. 6b, and the red line is the mean ion energy $\langle\varepsilon\rangle(t)$. To calculate the power in the ion beam, we now weight these average ion energies by the total current density collected by the FP over time. We show this resulting time resolved beam power in Fig. 7. We then calculate the time-averaged beam power as

$$P_{beam} = f_{rep}\int_0^{1/f_{rep}} I_b(t)\langle\varepsilon\rangle(t)dt. \tag{24}$$

For the pulsed mode the resulting ion beam power is 217 ± 15 W. And finally, we calculate the plasma efficiency according to Eq. 13 resulting in 13.5 ± 1.8% for the CW mode and 7.6 ± 1.1% for the pulsed mode.

While plasma efficiency is still the lowest component efficiency, the increase here is the largest percent increase between the two operational modes. The reason for this can be seen by examining the IEDF's in Fig. 6. In the CW mode, the thruster is able to accelerate ions consistently through an average 35 V potential drop. In the pulsed mode, the fastest ions—which arrive at the the probe first—are accelerated to similar energies (30 eV max). However, much of the beam is significantly less energetic with a tail decaying over time, ending in the single volt range. This tells us that the pulsed mode is not able to apply increased force due to self and structure field effects (See Ref. [10]), and that in fact the acceleration mechanism is hampered by the increased plasma density inherent to this mode.

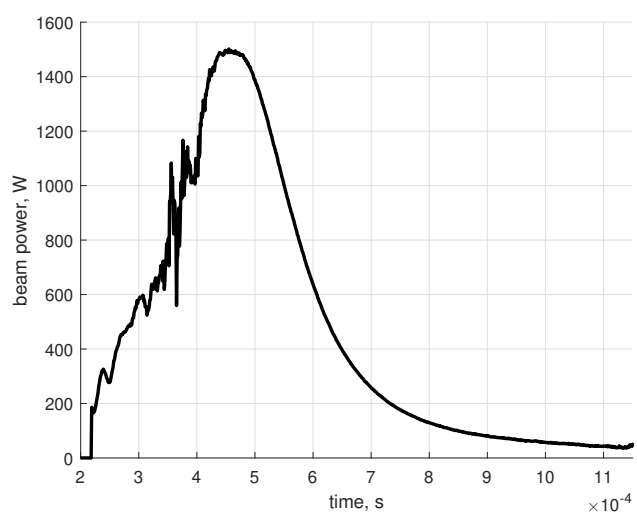

Fig. 7 Ion beam power for the pulsed mode as a function of time as collected by the far-field diagnostic probes.

V. Discussion

We represent the results presented above in a graphical format in Fig. 8(a). From the chart, we can see that the performance improves for the CW mode across all efficiency modes. This results in an overall probe measured efficiency (per Eq. 9) of 0.51 ± 0.02% for the pulsed mode and 2.9 ± 0.2% for the CW mode. We note these measurements generally agree with the thrust-stand measured efficiency (Shown for comparison in Fig. 8(b) and reproduced from

Ref. [11]), however we note the probe-measured efficiencies in both modes over predict the thrust-stand-measured efficiencies. This can be likely be attributed to the RPA measurements not being corrected for the local plasma potential.

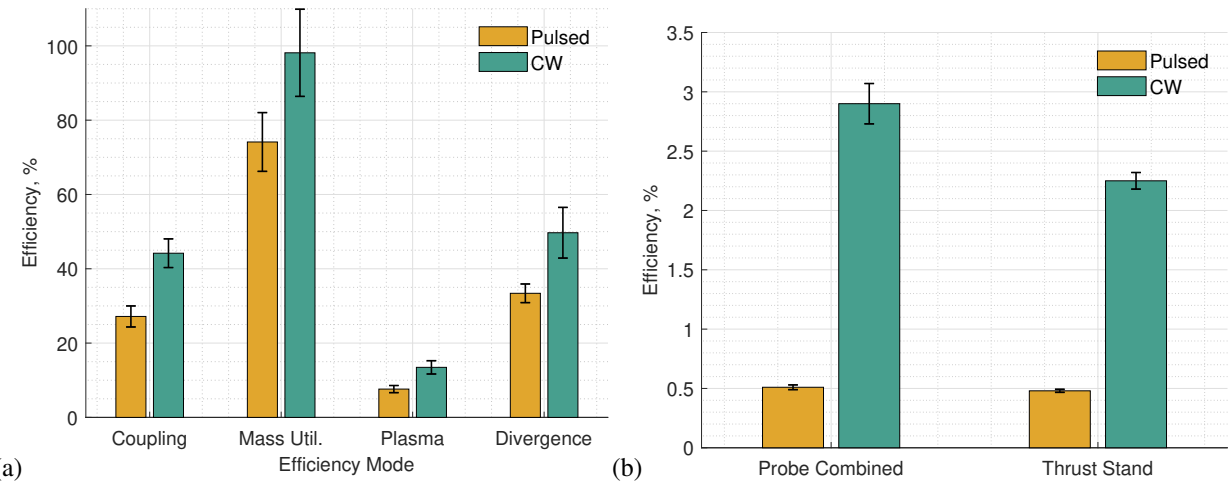

Fig. 8 (a) Phenomenological efficiency breakdowns for pulsed and CW mode (b) left: total efficiency from product of probe measurements, right: thrust stand measured efficiency.

Notably, the largest improvement—in terms of relative increase—comes from the plasma efficiency. Indeed, the CW operation increases this metric by a multiplicative 177%. This result lends further credence to the interpretation presented by Gill et al. [6] that the RMF drive scheme is not able to effectively directly couple to the plasma as is the case for theta-pinch and PIT thrusters. However, even with the performance improvements for the CW mode, the plasma efficiency clearly remains the largest loss mode for the thruster. This is easily understood through the results shown in Fig. 6. The low acceleration potentials measured (30 - 40 V) are not sufficient to evacuate the plasma from the thruster before it has a chance to lose energy through collisional processes—such as by interacting with the thruster wall.

To achieve a high plasma efficiency at this power and flow rate, the thruster would need to produce a potential drop for the ions an order of magnitude larger, on the order of 200 - 300 V (See Eq. 13). The simple way to improve this metric would be to increase the radial component of the applied magnetic field, as illustrated in Eq. 7. However, we see experimentally that increasing the strength of the applied magnetic field results in a steep decline in performance above some critical value [12]. Particularly in the CW mode, the thruster will not ignite if the applied magnetic field is too strong. We can interpret this effect through the lens of Eq. 5. The denominator in this expression tells us that as the applied magnetic field is increased the electron fluid will become increasingly magnetized to that field and will have a diminished response to the RMF. Ultimately, this results in a substantial reduction in azimuthal current drive in addition to reduced thruster performance.

If we embrace the CW operational mode for RMF thrusters, we can design two mitigation strategies to overcome this issue and accelerate the ions more effectively. First, with the reduction in current amplitude for the CW mode, we can improve the strength of the RMF through the use of additional antenna turns or ferromagnetic cores. This has the side effect of increasing antenna inductance which requires more voltage to drive, however the overall lower currents relative to the pulsed mode affords this to some level. Second, the axial component of the applied magnetic field is possibly less important for plasma confinement than it is in the pulsed mode. In the pulsed mode, the axial field is necessary to compress the plasma to keep it confined. However, with a reduction in plasma density in the CW mode, there is less internal magnetic pressure from the plasma to counteract. In this case, it may be beneficial to utilize all the applied magnetic field—which impedes current drive regardless of direction—in the radial direction where it can work to accelerate the ions. With these two changes, the geometry of future RMF thrusters may diverge substantially from the conical magnetic-nozzle shape from ELF heritage [4], and instead morph towards shorter coaxial configurations where the RMF and radial bias field can both be maximized.

VI. Conclusion

In this work, we have evaluated the performance of a rotating magnetic field thruster operating in pulsed and continuous wave mode. The pulsed mode consists of high amplitude RMF applied for 200 μs at a 7.8% duty cycle.

Conversely, the CW mode consists of sustained RMF application at roughly one quarter the amplitude of the pulsed mode. For the same power, flow rate, and applied magnetic field, we found that the efficiency of the thruster is substantially improved for the CW mode by approximately 400%.

To improve our understanding of this finding, we performed measurements of phenomenological efficiency modes: coupling efficiency, divergence efficiency, mass utilization, and plasma efficiency. We find that on average the CW mode improves all of these metrics by a multiplicative factor of 155%. Importantly, the largest improvement stems from the plasma efficiency which increases from 7.6% in the pulsed mode to 13.5% in the CW mode. This is additional evidence towards the hypothesis that RMF thrusters operating in pulsed mode are inherently inefficient. Any thruster operating in pulsed mode is subject to high plasma density directly resulting from the high density of slow pre-pulse neutrals. Because RMF thrusters are unable to directly apply force to the plasma through their antenna currents—contrary to other inductive pulsed plasma thrusters—, this high density does not serve to increase plasma acceleration. Instead the dense plasma only leads to enhanced collisional losses within the thruster resulting in inefficient operation.

Despite the improvements made in CW mode, overall RMF thruster efficiency remains below state-of-the-art for electric propulsion at roughly 3% jet efficiency (including power supply losses). However, a specific design focus on this operational regime may provide additional performance enhancements, as the thruster, and in-particular the power system, was constructed to run in both modes for this work. We believe that the CW mode for RMF thrusters, with improvements to the RMF strength and applied magnetic field, is the correct avenue to improve performance for this technology as this mode fully embraces the unique continuous directed current drive of RMF coupling.

Acknowledgements

This work was supported in part by NSTGRO Fellowship grant Number 80NSSC20K1168, NSTRF Fellowship grant number 80NSSC18K1190, and the AFOSR Space Propulsion and Power Program grant number FA9550-19-1-0022.

References

[1] Polzin, K. A., Martin, A. K., Eskridge, R. H., Kimberlin, A. C., Addona, B. M., Devineni, A. P., Dugal-Whitehead, N. R., and Hallock, A. K., *Summary of the 2012 Inductive Pulsed Plasma Thruster Development and Testing Program*, NASA-Marshall Space Flight Center, Huntsville, AL, 2013. No. NASA/TP-2013-217488.

[2] Sun, Y., Levchenko, I., Lim, J. W., Xu, L., Huang, S., Zhang, Z., Thio, F., Potrivitu, G. C., Rohaizat, M. W., Cherkun, O., Chan, C. S., Baranov, O., Bazaka, K., and Xu, S., "Miniaturized rotating magnetic field-driven plasma system: Proof-of-concept experiments," *Plasma Sources Science and Technology*, Vol. 30, 2021. https://doi.org/10.1088/1361-6595/ab9b34.

[3] Furukawa, T., Kuwahara, D., and Shinohara, S., "Spatial characteristics of rotating magnetic field (RMF) plasma acceleration method in open magnetic field configuration under partial RMF penetration," *Physics of Plasmas*, Vol. 28, 2021. https://doi.org/10.1063/5.0035383.

[4] Weber, T. E., "The Electrodeless Lorentz Force Thruster Experiment," *Thesis*, 2010. University of Washington.

[5] Sercel, C. L., Gill, T., Woods, J. M., and Jorns, B., "Performance Measurements of a 5 kW-Class Rotating Magnetic Field Thruster," *AIAA Propulsion and Energy Forum*, 2021. https://doi.org/10.2514/6.2021-3384.

[6] Gill, T. M., Sercel, C. L., and Jorns, B. A., "Experimental investigation into efficiency loss in rotating magnetic field thrusters," *Plasma Sources Science and Technology*, 2023.

[7] Sercel, C. L., Gill, T., and Jorns, B., "Performance Predictions for CW-Mode Operation of an RMF Thruster," American Institute of Aeronautics and Astronautics (AIAA), 2023. https://doi.org/10.2514/6.2023-0449.

[8] Su, L. L., Roberts, P. J., Gill, T., Hurley, W., Marks, T. A., Sercel, C. L., Allen, M., Whittaker, C. B., Byrne, M., Brown, Z., et al., "Operation and Performance of a Magnetically Shielded Hall Thruster at Ultrahigh Current Densities on Xenon and Krypton," *AIAA SCITECH 2023 Forum*, 2023, p. 0842.

[9] Brown, D. L., Walker, M. L. R., Szabo, J., Huang, W., and Foster, J. E., "Recommended practice for use of faraday probes in electric propulsion testing," *Journal of Propulsion and Power*, Vol. 33, 2017, pp. 582–613. https://doi.org/10.2514/1.B35696.

[10] Sercel, C. L., Gill, T. M., and Jorns, B. A., "Inductive probe measurements in a rotating magnetic field thruster," *Plasma Sources Science and Technology*, 2023.

[11] Sercel, C. L., Gill, T., and Jorns, B., *Performance Measurements of a 10-kw class RMF Thruster*, 2023. (In preparation).

[12] Sercel, C. L., "Characterization of Performance and Current Drive Mechanism for the Rotating Magnetic Field Thruster," *Thesis*, 2023. University of Michigan.